Visnyk NTUU KPI Seriia – Radiotekhnika Radioaparatobuduvannia, 2019, Iss. 77, pp. 17–29

The Analysis of Energy Transition Processes in Boost Converter

Martynyuk V. V., Kosenkov V. D., Geydarova O. V., Fedula M. V.

Khmelnytskyi National University

E-mail: *fedula@khnu.km.ua*

Introduction. This article presents the analysis of energy transition processes in boost converter under the conditions of load changing. The boost converter laboratory layout is investigated with forms of the transient process caused by load changing. The transient currents and voltages are measured in harmonic and anharmonic modes. The parameters of boost converter transient modes are estimated. The analysis of energy transition processes is performed using two boost converter models.

Problem statement. The boost converter circuits are used in the areas of electronics where the minimization of energy losses is strictly required. The boost converter energy losses depend on the form of transient processes caused by load changing. The purpose of energy losses minimization requires exact analysis of energy transition processes which appear under load changing. The presented work describes the responses of boost converter circuit to changing the load twice with four different transient modes.

Results. The analysis of energy transition processes is performed with two models. The first model is based on the iterative mapping technique, where the currents and voltages of each period of gate driving signal are determined from the circuit parameters and initial conditions given by the previous period of driving signal. Such model allows to perform an exact analysis of current and voltage ripple transient processes. But the iterative mapping model is characterized by numerical approximation errors and requires more computation time. The second model describes the envelopes of boost converter current and voltage transient processes analytically. This model is based on the state-space averaging method which is widely used for modelling of switching circuits. Such model does not take into account the waveforms of current and voltage ripples, but it provides a more simple description of transient process envelopes which are useful for the circuit design purposes. The modeling results obtained from iterative mapping and state space averaging, match with the experimental data.

Conclusions. The performed analysis shows that the energy losses depend on the transient process mode significantly. During the load transient process time, the smallest energy losses can be obtained under the critical load transient process form which is situated between periodic and aperiodic modes. Such result is obtained experimentally and confirmed by the both iterative mapping and state-space averaging models. The analytical results are confirmed by optimization procedure in MATLAB environment.

Key words: boost converter; energy losses; transient process; critical mode; modelling

DOI: 10.20535/RADAP.2019.77.17-29

Introduction

The boost converters are used in many fields of modern electronics [1–3]. Mostly, boost converters function as sources and converters in power supplies of different electrical devices [3, 4]. There are many different circuit realizations of boost converters [2,3,5–9]. But the main principles of DC-to-DC power conversion with output voltage increase correspond to the basic circuit [3, 10, 11] that is shown in Fig. 1, where the capacitor voltage is increased regarding to the inductor that functions as a current source.

The analysis of transient processes and minimization of energy losses in boost converter circuits are important problems of modern power systems research [3, 12]. Such problems appear, for an example, in renewable energy sources [4,13,14], smart grids [14,15], and other devices with high requirements to energy consumption [2, 16, 17]. Also, one of most important boost converter application areas is the photovoltaic energetics [4, 18–20]. The work [21] shows that the photovoltaic battery exploitation efficiency can be improved significantly by using optimizer circuit based on a boost converter. The new directions of boost converter research are related to the investigation of its transient responses under different control forms [20, 22–28]. Various models of boost converters are investigated due to the practical application features [29–34]. So, in these works the fractional order models for DC-DC converters and other circuits are analyzed in accordance with parameters of real electrical parts. One of the most important fields of boost converter development is the analysis of transient responses

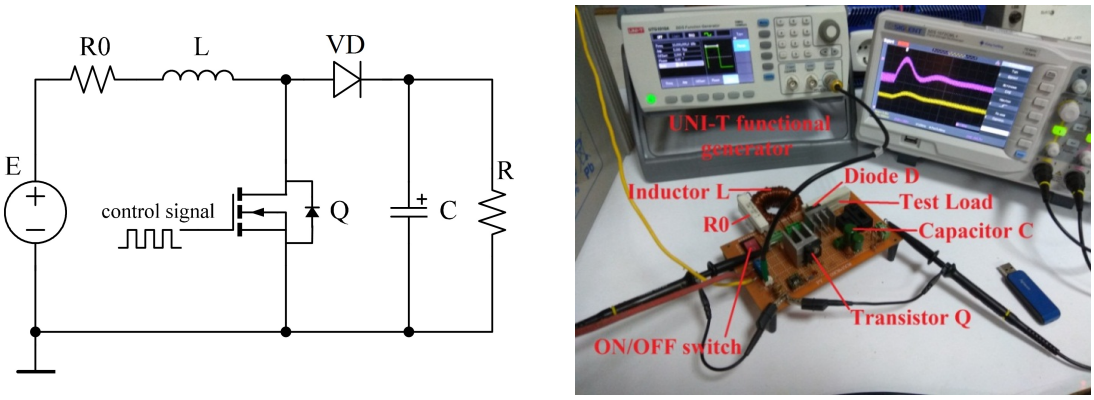

(a) (b)

Fig. 1. The boost converter circuit diagram (a) and laboratory realization (b)

under varying load [4,13,17,26]. Thus, it causes transient processes that influence the loss characteristics.

In this paper the analysis of boost converter losses and responses to load transients is performed using analytical techniques and optimization procedure based on iterative mapping models.

1 The Considered Boost Converter

The boost converter circuit diagram [3,11,28] and its realization are shown in Fig. 1.

In the presented work, the boost converter is realized on the base of $2mH$ inductor with magnetodielectric core (sendust, $\mu_0 = 60$) and electrolytic capacitors with ESR $< 70m\Omega$ and parasitic inductance less than $10\mu H$. The switch is designed on the base of power MOSFET transistor STW88N65M5 [35]. The rectifier VD is power Shottky diode 30CPQ150 [36]. The source voltage is $E = 12.87V$. A significant parasitic resistance is modelled by resistor $R_0 = 1\Omega$. The converter is investigated with load resistances 25Ω, 50Ω, 100Ω. The driving signal is generated by UNI-T UTG1010A functional generator.

The more detailed specifications of designed boost converter elements are presented in Table 1.

Such elements are selected for achieving a wide range of experimental modes and more exact analysis of different boost converter modeling techniques.

2 The Boost Converter Modelling

The boost converter circuit (Fig. 1) can be represented by two equivalent circuits [3] for open and closed MOSFET switch that is shown in Fig. 2.

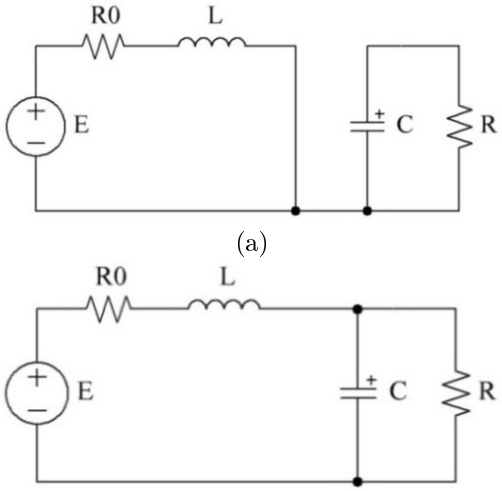

(a)

(b)

Fig. 2. The equivalent circuit: (a) the switch is closed; (b) the switch is open

In the state 1 the inductor current increases up to the maximum value that is defined by parasitic resistance R_0. The capacitor is discharged to the load resistance R. Such as the boost converter is separated into two first-order circuits, the transient processes have exponential form in the state 1. Accordingly to the state-space averaging method [3,11,31,37,38], the boost converter (Fig. 1) model can be represented in the form (1).

$$\begin{bmatrix} L\frac{di_L}{dt} \\ C\frac{dv_C}{dt} \end{bmatrix} = \begin{bmatrix} -R_0 & -(1-D) \\ (1-D) & -\frac{1}{R} \end{bmatrix} \times \begin{bmatrix} i_L \\ v_C \end{bmatrix} + \\ + \begin{bmatrix} 1 \\ 0 \end{bmatrix} \times \begin{bmatrix} E \\ 0 \end{bmatrix}, \quad (1)$$

where t is the time L is the inductance, C is the capacitance, E is the source voltage, R is the load resistance, i_L is the inductor current, v_C is the capacitor voltage, D is the duty cycle of switching (Fig. 1). The model (1) allows to obtain averaged voltage and current transient processes waveforms. For more exact modelling with

Table 1 The main parameters of the designed boost converter (Fig. 1) elements

Parts	Parameter	Value
Inductor L	inductance	2 mH
	magnetic core material	sendust
	Magnetic core material parameters:	
	initial magnetic permeability μ_0	60
	eddy current loss coefficient	$250 \cdot 10^{-9}$ 1/Hz
	hysteresis loss coefficient	$5 \cdot 10^{-3}$
	additional loss coefficient	$2 \cdot 10^{-3}$
	the operation frequency range	10 kHz
	maximum loss angle tangent	0.01
Capacitors C	capacitances	8mF, 40µF, 2.1mF, 1.94mF
	maximum ESR at 10kHz	70 mΩ
	maximum equivalent inductance	10 µH
Diode VD	part number	30CPQ150
	type	Shottky
	repetitive peak reverse voltage V_{RRM}	150 V
	maximum average forward current $I_{F(AV)}$	30 A
Transistor Q	part number	STW88N65M5
	type	MOSFET
	maximum drain-to-source voltage V_{DSS}	710 V
	drain current I_D	84 A
	maximum drain-source on resistance $R_{DS(on)}$	29 mΩ

accounting of current and voltage ripple, the boost converter behaviour can be described by the iterative mapping (2) and (3) expressed in accordance with [1–3, 39]. The inductor current is determined by (2):

$$i_L(t) = \begin{cases} \frac{E}{R_0} - \frac{E}{R_0} e^{-\frac{R_0}{L}(t-t_k)} + \\ \quad + i_L(t_k) e^{-\frac{R_0}{L}(t-t_k)}, \quad \text{state 1} \\ \left(A_0 + A_1 e^{p_1(t-t_k)} + A_2 e^{p_2(t-t_k)}\right) E + \\ \left(A_3 e^{p_1(t-t_k)} + A_4 e^{p_2(t-t_k)}\right) i_L(t_k) + \\ \left(A_5 e^{p_1(t-t_k)} + A_6 e^{p_2(t-t_k)}\right) v_C(t_k), \\ \quad \text{state 2.} \end{cases} \quad (2)$$

The capacitor voltage is determined by (3):

$$v_C(t) = \begin{cases} v_C(t_k) \cdot e^{-\frac{1}{R_H C}(t-t_k)}, \quad \text{state 1} \\ \left(B_0 - B_1 e^{p_1(t-t_k)} - B_2 e^{p_2(t-t_k)}\right) E + \\ \left(B_3 e^{p_1(t-t_k)} + B_4 e^{p_2(t-t_k)}\right) i_L(t_k) + \\ \left(B_5 e^{p_1(t-t_k)} + B_6 e^{p_2(t-t_k)}\right) v_C(t_k), \\ \quad \text{state 2} \\ v_C(t_k) e^{-\frac{1}{R_H C}(t-t_k)}, \quad \text{state 2,} \\ \quad i_L(t) = 0 \ (t_k \text{ is the time when} \\ \quad i_L(t) \text{ reaches value 0}), \end{cases} \quad (3)$$

where t is the time, t_k is the time of the last commutation to state 1, k is the number of the last commutation, E is the electromotive force of the voltage source, L is the inductance, R is the load resistance. The coefficients A_n and B_n $(n = 0, 1, 2, 3, 4, 5, 6)$ are defined by the following expressions:

$$\begin{array}{ll} A_0 = \frac{d}{c} & B_0 = 1 - A_0 R_0 \\ A_1 = \frac{d}{2c}\left(-1 - \frac{b}{Q}\right) + \frac{1}{QL} & B_1 = (R_0 + Lp_1) A_1 \\ A_2 = \frac{d}{2c}\left(-1 + \frac{b}{Q}\right) - \frac{1}{QL} & B_2 = (R_0 + Lp_2) A_2 \\ A_3 = \frac{1}{2}\left(1 + \frac{b}{Q}\right) + \frac{R0}{QL} & B_3 = (R_0 + Lp_1) A_3 \\ A_4 = \frac{1}{2}\left(1 - \frac{b}{Q}\right) - \frac{R0}{QL} & B_4 = (R_0 + Lp_2) A_4 \\ A_5 = \frac{1}{QL} & B_5 = (R_0 + Lp_1) A_5 \\ A_6 = -\frac{1}{QL} & B_6 = (R_0 + Lp_2) A_6 \end{array}$$

where b and c are the state 2 characteristic equation (4) coefficients, which are defined as follows:

$$b = \frac{RR_0C + L}{RLC}, \quad c = \frac{R + R_0}{RLC}, \quad s^2 + b \cdot s + c = 0. \quad (4)$$

Q is the square root of characteristic equation discriminant, i.e. $Q = \sqrt{b^2 - 4c}$, where s is the complex frequency, and the coefficient d is defined as $d = 1/(RLC)$. The characteristic equation (4) roots are$p_1 = (-b + Q)/2$, and $p_2 = (-b - Q)/2$. In the state 2, the dynamics of transient processes depend on the values of the roots $p_1$and p_2. If the roots are real numbers, then the inductor current $i_L(t)$ and capacitor voltage $v_C(t)$ change with time by exponential laws that correspond to (4). If the roots p_1 and p_2 are complex $(4c > b^2)$, then the transient processes are damping harmonic oscillations. The roots of characteristic equation are

$$p_{1,2} = -\delta \pm j\omega_f, \quad (5)$$

where $\delta = b/2$, $\omega_f = \sqrt{b^2/4 - c}$. In such case, the inductor current and capacitor voltage include harmonic components:

$$i_L(t) = E/(R_0 + R) + Ge^{-\delta t} \cdot \sin(\omega_f t + \psi), \quad (6)$$

$$v_C(t) = E + Ge^{-\delta t} \cdot \cdot \cos\left(\omega_f t - (R_0 - \delta L)/(L\omega_f)\right) \cdot \cdot \sqrt{(L\omega_f)^2 + (\delta L - R_0)^2}, \quad (7)$$

where G is the amplitude of harmonic oscillations.

3 The Approximate Calculation of Boost Converter Parameters

If the ripple level is low and transient processes have the form of almost straight lines, then the parameters of boost converter can be obtained by approximate techniques related to the ones described in [3]. Some of such techniques are presented below.

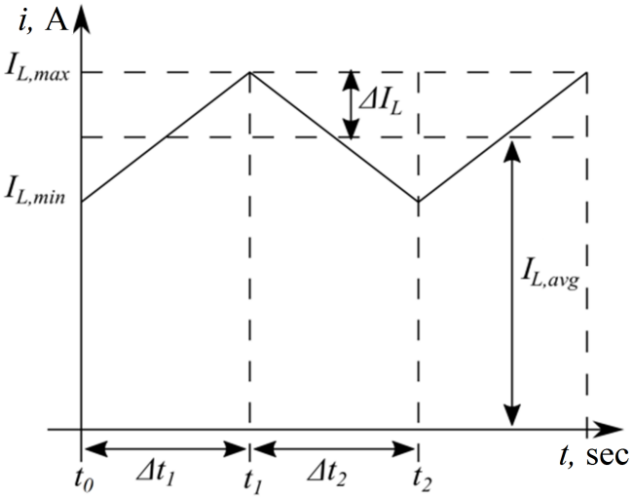

a

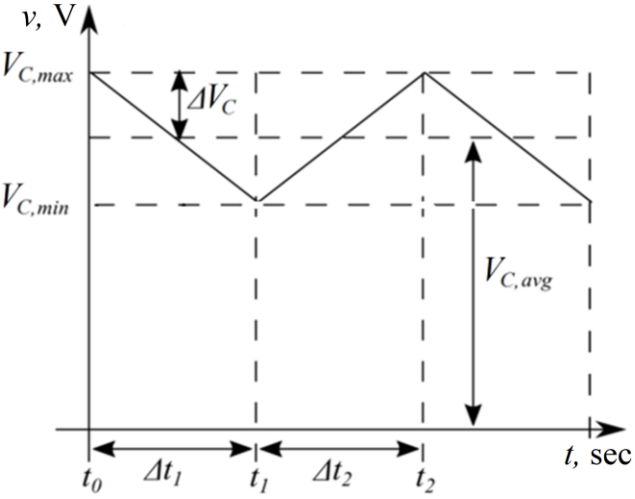

b

Fig. 3. Almost linear form of inductor current (a) and capacitor voltage (b) transients

If the forms of inductor current and capacitor voltage transients are almost linear (Fig. 3), then the initial conditions for **the** state 1 are given by the expressions:

$$\begin{cases} i_L(t_0) = I_{L,\min} = I_{L,avg} - \Delta I_L, \\ v_C(t_0) = V_{C,\max} = V_{C,avg} + \Delta V_C, \end{cases} \quad (8)$$

where $I_{L,avg}$ is the averaged inductor current, $V_{C,avg}$ is the averaged capacitor voltage, ΔI_L and ΔV_C are the ripple estimations, t_0, t_1, t_2 are the commutation time moments, accordingly to Fig. 3.

Therefore, the initial conditions for the state 2 are defined by the following expression:

$$\begin{cases} i_L(t_1) = I_{L,\max} = \dfrac{E}{R_0} + \\ \qquad + \left(I_{L,\min} - \dfrac{E}{R_0}\right) e^{-\frac{R_0}{L}(t_1 - t_0)} \\ v_C(t_1) = V_{C,\min} = v_C(t_0) \cdot e^{-\frac{t_1 - t_0}{RC}}. \end{cases} \quad (9)$$

The periods of the state 1 and state 2, Δt_1 and Δt_2 (Fig. 3) can be obtained from the conditions for the ripple of inductor current (ΔI_L) and capacitor voltage (ΔV_C). If we set $\Delta I_L = K_1 \cdot I_{L,avg}$, where K_1 is a real positive coefficient, then, for $t = t_1$, the inductance current is determined by (10):

$$i_L(t_1) = I_{L,avg} + K_1 \cdot I_{L,avg} = = E/R_0 + (I_{L,\min} - E/R_0)\, e^{-\frac{R_0}{L}\Delta t_1}. \quad (10)$$

The above expressions allow to obtain the equation (11).

$$e^{-\frac{R_0}{L}\Delta t_1} = \frac{I_{L,avg} + K_1 I_{L,avg} - E/R_0}{I_{L,avg} - K_1 I_{L,avg} - E/R_0}, \quad (11)$$

which provides the state 1 duration Δt_1 given by the following formula:

$$\Delta t_1 = -\frac{L}{R_0} \ln \frac{(1 + K_1) I_{L,avg} - E/R_0}{(1 - K_1) I_{L,avg} - E/R_0}. \quad (12)$$

The averaged capacitor voltage can be determined using [26, 31, 33] for $R_0 = 0$:

$$V_{C,avg} = K_\delta \cdot E, \quad (13)$$

where $K_\delta = (\Delta t_1 + \Delta t_2)/\Delta t_1$. The averaged current $I_{ld,avg}$ and power $P_{ld,avg}$ values are given by (14):

$$I_{ld,avg} = V_{C,avg}/R, P_{ld,avg} = V_{C,avg}^2/R. \quad (14)$$

Besides, we can use a more exact formula for averaged load power:

$$P_{ld,avg} = \frac{1}{T} \int_0^T \frac{(v_C(\tau))^2}{R} d\tau, \quad (15)$$

but a simple analysis shows small error under $\Delta t_1 = \Delta t_2 = T/2$, where T is the period of commutation.

Such as at the state 1, we obtain $V_C = v_C(t_0) - 4\Delta V \cdot t/T$, then, during the time $T/2$, the averaged load power is

$$P_{ld,avg} = \\ = \frac{1}{T/2}\int_0^{T/2} \frac{(V_{C,\max} - 4\Delta V \cdot t/T)^2}{R} dt = \\ = \frac{1}{R}(V_{C,avg}^2 + \frac{1}{3}\Delta V^2). \quad (16)$$

For instance, if the ripple ΔV is limited by condition $\Delta V = 0,1V_{C,avg}$ (voltage oscillation level is significant), then the error is only 0.33%, due to (17). Thus, for $R_0 = 0$ obtain

$$P_s = P_{ld} \quad \text{or} \quad E \cdot I_{L,avg} = V_{C,avg} \cdot I_{ld,avg} \quad (17)$$

and the inductor current is $I_{L,avg} = I_{ld,avg} \cdot V_{C,avg}/E = I_{ld,avg} \cdot K_\delta \cdot E/E = K_\delta \cdot I_{ld,avg}$.

So, the boost converter circuit is a step-up transformer with transformation coefficient K_δ.

$$\frac{V_{C,avg}}{E} = \frac{I_{L,avg}}{I_{ld,avg}} = K_\delta. \quad (18)$$

Now, let's analyze the influence of resistance R_0 on the averaged values of capacitor voltage $V_{C,avg}$ and inductor current $I_{L,avg}$. If $R_0 \neq 0$, then equivalent source voltage is

$$V_s = E - I_{L,avg} \cdot R_0 \quad (19)$$

and the load voltage is defined by (20):

$$V_{C,avg} = K_\delta \cdot (E - I_{L,avg} \cdot R_0) = \\ = K_\delta(E - K_\delta \cdot I_{ld,avg} \cdot R_0) = \\ = K_\delta(E - K_\delta V_{C,avg} R_0/R). \quad (20)$$

Hence, the averaged load voltage $V_{C,avg}$ and averaged load current $I_{ld,avg}$ are determined by the following expressions:

$$V_{C,avg} = K_\delta \cdot E/(1 + K_\delta^2 R_0/R), \quad (21)$$

$$I_{ld,avg} = V_{C,avg}/R. \quad (22)$$

Thus, the averaged inductor current is

$$I_{L,avg} = K_\delta \cdot V_{C,avg}/R = \\ = (K_\delta/R) \cdot K_\delta E/(1 + K_\delta^2 R_0/R). \quad (23)$$

Such as $V_{C,\min} = V_{C,\max} e^{-t/(RC)}$, then we obtain the following expression for the state 1 duration:

$$\Delta t_1 = -RC \ln\left(\frac{V_{C,avg} - \Delta V}{V_{C,avg} + \Delta V}\right). \quad (24)$$

If we consider the voltage ripple $\Delta V = 0.1 \cdot V_{C,avg}$ and state 1 transient process time constant $RC = 2.5 \cdot 10^{-4}$ sec, then we obtain $\Delta t_1 = 5 \cdot 10^{-5}$ sec from the formula (24). On the other hand, let's determine the parasitic resistance R_0 value that makes boost converter losing advantages in comparison with direct load-to-source connection, i.e. $V_{C,avg} > E \cdot R/(R_o + R)$ or

$$K_\delta E/(1 + K_\delta^2 \cdot R_0/R) > E \cdot R/(R_0 + R). \quad (25)$$

After several transformations of expression (25), we obtain the condition:

$$R_0 < R/K_\delta. \quad (26)$$

If $R_0 = R/K_\delta$, then the boost converter load voltage is equal to the voltage of direct load-to-source connection. For the state 2, the boost converter circuit must satisfy the condition $\Delta t_2 << 2\pi/\omega_f$ to avoid high losses and load voltage distortions. The performed analysis and measurements show, that under $\Delta t_1 = \Delta t_2 = 2\pi/\omega_f > 3 \cdot RC$, the capacitor discharges almost to zero, and we can consider $V_{C,\min} = 0$. Then, $V_{C,avg} = V_{C,\max}/2$. Thus, for the selection of capacitance C, we can set the condition $\Delta t_2 = \Delta t_1 = RC/(5...10)$. The value of K_δ can be obtained from the following condition:

$$\frac{dv_C}{dK_\delta} = \frac{d}{dK_\delta}\left(K_\delta E/(1 + K_\delta^2 R_0/R)\right) = 0, \quad (27)$$

hence, we obtain the transformation coefficient:

$$K_\delta = \sqrt{R/R_0} \quad (28)$$

4 The Analysis of Boost Converter Transient Process Modes Under Varying Load

The boost converter models and laboratory layout are investigated with the parameters $E = 12.87V$, $L = 2mH$, $R_0 = 1\Omega$, $\Delta t_1 = \Delta t_2 = 5 \cdot 10^{-5}$ sec for load resistances 25Ω, 50Ω, 100Ω. The capacitance C impacts the boost converter transient process mode. It is obtained by four different techniques in subsections 4.1 – 4.4, respectively.

4.1 The Critical Transient Process in the State 2 (Switch Off)

The aperiodic and periodic modes of capacitor charging are considered for fixed values of E,L,R_0,R. If the characteristic equation (4) has a single solution $p_{1,2} = -\delta$, then the critical capacitor charging mode appears. The critical mode condition is defined by (29):

$$(L + R_0 RC)/(2RLC) = (R_0 + R)/(RLC). \quad (29)$$

The solution of the equation (29) gives the following result:

$$C = \frac{L}{{R_0}^2 R}\left[(R_0 + 2R) + 2\sqrt{R_0 R + R^2}\right]. \quad (30)$$

Thus, the capacitance value (30) provides the critical form of state 2 transient process. Whereas, for periodic charging mode, the inequality (31) must be satisfied:

$$C < \frac{L}{{R_0}^2 R}\left[(R_0+2R)+2\sqrt{R_0R+R^2}\right]. \quad (31)$$

For the presented boost converter parameters, state 2 critical capacitance (30) is 8 mF.

In Fig. 4, the load transient processes are shown for the load resistance changing from initial value $R_{init} = 50\Omega$ to $R = 25\Omega$ (triangle markers) and to $R = 100\Omega$ (square markers). The left plots show the ranges of experimental and modeled boost converter transient current and voltage. Right plots show the respective current and voltage ripple waveforms for the load resistances $R = 25\Omega$ and $R = 100\Omega$. Also, the ripple waveforms are plotted for the case, when the load transient is absent and the resistance remains still $R = R_{init} = 50\Omega$ (circular markers). The final values of load resistance are denoted in the figure legend. The next plots Fig. 5, Fig. 6, Fig. 7 are organized in the same way.

4.2 The Maximum Voltage Boost Mode

The following analysis is performed for obtaining the capacitance value, that provides the maximum speed of periodic capacitor charging. The boost converter circuit is connected to the voltage source E under the initial conditions: $i_L(0) = 0$, $v_C(0) = 0$. Under $p_{1,2} = -\delta \pm j\omega$ we obtain

$$\begin{cases} v_C = \dfrac{ER}{R_0+R} + Ge^{-\delta t}\sin(\omega_f t+\psi), \\ i_C = CGe^{-\delta t}\left(-\delta(\sin\omega t+\psi)+\omega\cos(\omega t+\psi)\right). \end{cases} \quad (32)$$

Next, the expressions (32) are simplified for $t = 0$, as follows.

$$\begin{cases} G\sin\psi = -ER/(R+R_0), \\ G\cos\psi = -(\delta/\omega_0)\cdot ER/(R+R_0), \end{cases} \quad (33)$$

where $tg\psi = \omega_f/\delta$, $\psi = arctg(\omega_f/\delta)$. On the other hand,

$$\begin{cases} \sin\psi = \omega_f/\sqrt{\omega_f^2+\delta^2} = \omega_f/\omega_0, \\ \cos\psi = \delta/\sqrt{\omega_f^2+\delta^2} = \delta/\omega_0, \end{cases} \quad (34)$$

$$G = (-ER/(R_0+R))/\sin\psi = \\ = -(\omega_0/\omega_f)\cdot E\cdot R\cdot/(R_0+R). \quad (35)$$

As a result, we obtain the expression for capacitor voltage:

$$v_C = \frac{ER}{R_0+R}\cdot\left(1-\frac{\omega_0}{\omega_f}e^{-\delta t}\sin(\omega_f t+\psi)\right). \quad (36)$$

The maximum value of the voltage u_C can be reached under $t = T_f/2$, i.e.

$$v_{C,}T_{f/2} = E\frac{R}{R+R_0}\times \\ \times\left[1+\exp\left(-\frac{\frac{L+R_0RC}{2RLC}}{\sqrt{\frac{R_0+R}{RLC}-\frac{(L+R_0RC)^2}{4R^2L^2C^2}}}\right)\right]. \quad (37)$$

The capacitance, that provides the maximum voltage $v_C$for $t = T_f/2$, can be defined by the differential equation

$$\frac{dv_{C,}T_{f/2}}{dt} = 0, \quad (38)$$

The solution of equation (38) is

$$C = L/(R_0R) \quad (39)$$

The maximum voltage boost condition (39) gives the capacitance value C=40μF.

Fig. 5 shows the respective transient processes where the load changes from 50 Ω to R, similarly to Fig. 4.

4.3 The Critical Averaged Envelope Transient Process Mode

The characteristic equation of state-space averaging model (1) is given by (40):

$$s^2+\frac{R_0RC+L}{RLC}s+\frac{R\cdot(D-1)^2+R_0}{RLC} = 0. \quad (40)$$

Thus, for the critical envelope transient process, the condition (41) must be satisfied.

$$\left(\frac{R_0RC+L}{RLC}\right)^2-4\frac{R\cdot(D-1)^2+R_0}{RLC} = 0. \quad (41)$$

From equation (41), the critical capacitance is obtained as (42).

$$C_{1,2} = \frac{L}{R_0^2R}\cdot\left(R_0+2R(1-D)^2 \right. \\ \left. \pm\sqrt{-R_0^2+\left(-R_0-2R(1-D)^2\right)^2}\right). \quad (42)$$

Such as C_2 reaches very low values (near 10^{-7}) under the given boost converter circuit parameters ($R_0 = 1\ \Omega$, $R = 50\ \Omega$, $L = 2$ mH, $D = \Delta t_1/(\Delta t_1+\Delta t_2) = 0.5$), then we select

$$C = C_1 = \frac{L}{R_0^2R}\cdot\left(R_0+2R(1-D)^2 \right. \\ \left. \pm\sqrt{-R_0^2+\left(-R_0-2R(1-D)^2\right)^2}\right). \quad (43)$$

The critical envelope mode capacitance C=2.1mF is obtained from (43).

Fig. 6 shows corresponding transient processes and ripples, where load changes from 25 Ω to 100 Ω value.

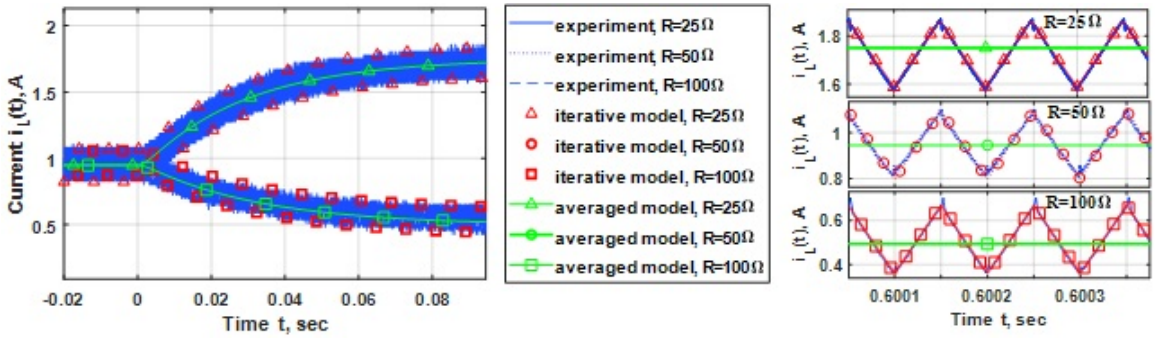

(a)

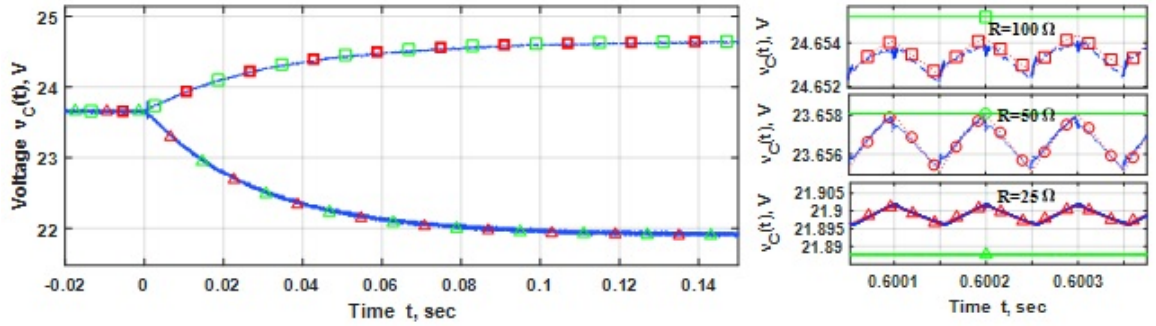

(b)

Fig. 4. The transient processes under state 2 critical capacitance C=8 mF: (a) inductor currents; (b) output capacitor voltages

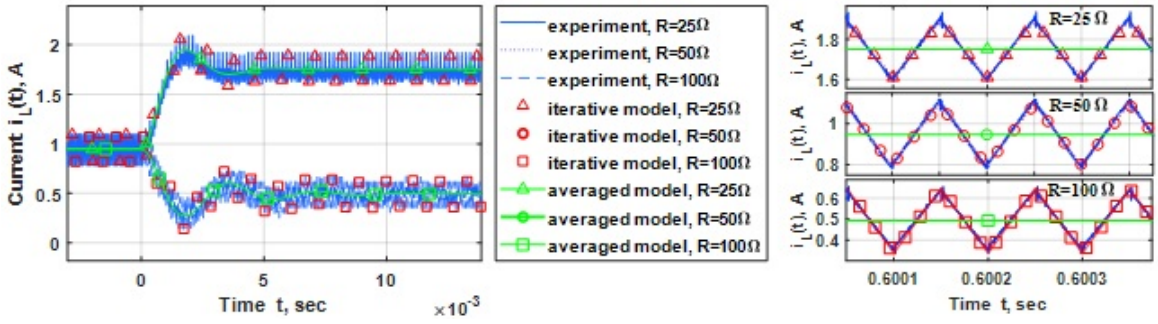

(a)

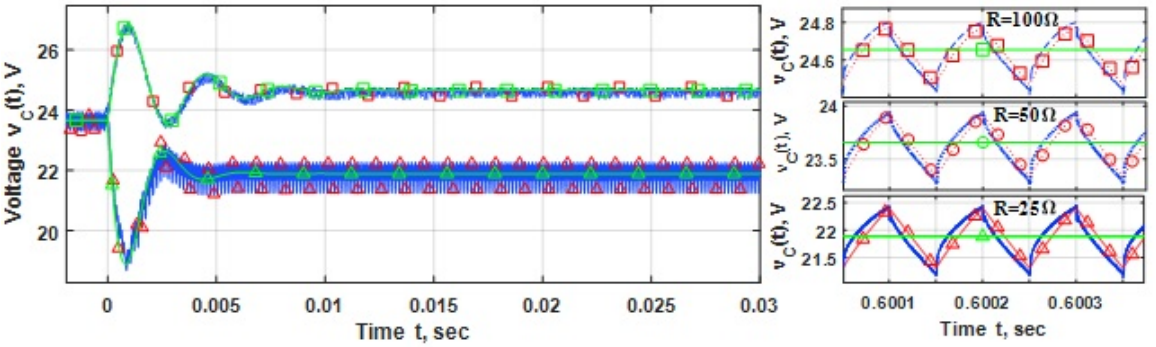

(b)

Fig. 5. The transient processes under maximum voltage boost capacitance C=40 µF: (a) inductor currents; (b) output capacitor voltages

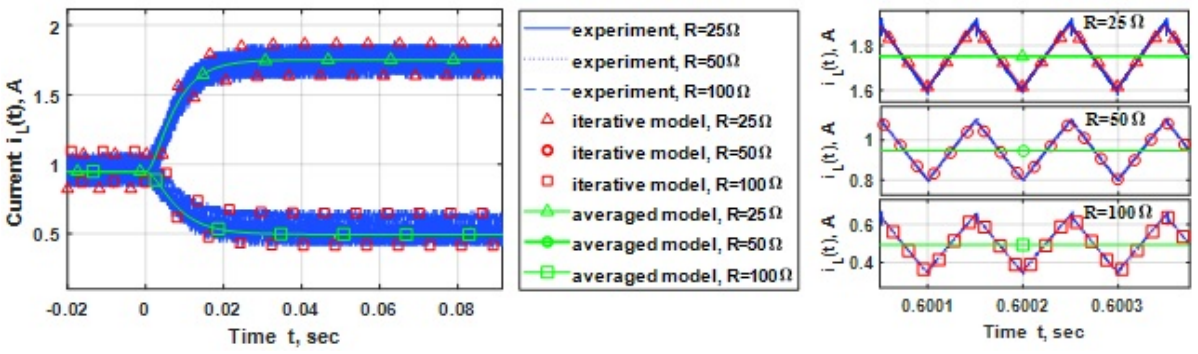

(a)

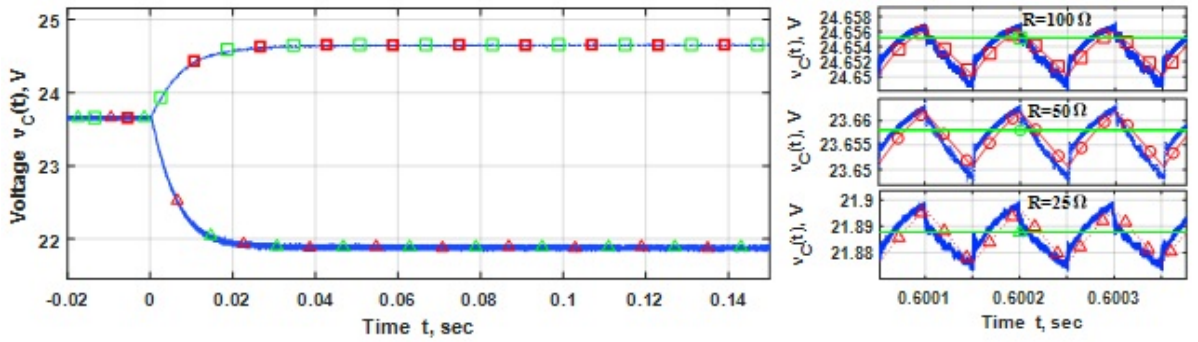

(b)

Fig. 6. The transient processes under critical envelope capacitance C=2.1mF: (a) inductor currents; (b) output capacitor voltages

4.4 The Optimized Transient Process Mode

In boost converter circuit, the losses are estimated by the input energy W_{in} and output energy W_{out}. The boost converter efficiency estimation is the maximum energy loss between the cases when the load resistance does not change ($R = 50\ \Omega$), when it decreases twice ($R = 25\ \Omega$) and when it increases twice ($R = 100\ \Omega$). Such estimation allows obtaining the best parameters for boost converter under the varying the load resistance in the given range $R = 50\ \Omega \pm 50\%$.

The input energy W_{in} is the energy that passes from voltage source with electromotive force E to the boost converter circuit from time t_1 to time t_2:

$$W_{in} = \int_{t_1}^{t_2} E \cdot i_L(\tau) d\tau. \tag{44}$$

Respectively, the output energy W_{ld} is the energy transmitted to load resistance:

$$W_{ld} = \int_{t_1}^{t_2} \frac{(v_C(\tau))^2}{R} d\tau. \tag{45}$$

The energy loss coefficient is given in per cents:

$$K_{loss} = 100 \cdot (W_{in} - W_{ld})/W_{in}. \tag{46}$$

The boost converter efficiency is estimated by the expression

$$K_{loss,\max} = \max(K_{loss,0}, K_{loss,1}, K_{loss2}), \tag{47}$$

where $K_{loss,0}$ is the loss coefficient for the initial resistance ($R_{ld,0} = 50\ \Omega$), $K_{loss,1}$ is the loss coefficient for the resistance $R_{ld,0}/2$, and $K_{loss,2}$ is the loss coefficient for the resistance $R = 2R_{ld,0}$.

Thus, the boost converter losses minimization problem can be represented as (48):

$$\min_C (\max(K_{loss,0}, K_{loss,1}, K_{loss2})), \tag{48}$$

under the condition $V_0 - \Delta V < v_C < V_0 + \Delta V$, where $\Delta V = 0.1 \cdot V_0, V_0 = 24\ V$.

The minimization procedure is performed in MATLAB environment using fmincon function. As the result, the capacitance C=1.94 mF is obtained.

The load transient processes and ripples are shown in Fig. 7.

5 The Comparison of Boost Converter Efficiency with Different Load Transient Process Modes

The boost converter losses (46), (47) are analyzed for the capacitances obtained from expressions (30), (39), (43) and (48) for the observation time $t \in [-T_{tr},\ T_{tr}]$ where T_{tr} is the duration of the longest of the investigated transient processes (for the capacitance 8 mF). In Table 2, the experimental

and modeled losses are presented with corresponding relative errors of modelling (the averaged envelope (1) is compared to the averaged experimental data). All modelling errors are calculated in per cents by the formula

$$\varepsilon(X) = 100 \cdot \frac{|X_{\text{exp}} - X_{model}|}{\max(X_{\text{exp}}) - min(X_{\text{exp}})}, \qquad (49)$$

where X_{exp} is the experimental value, X_{model} is a modeled value.

The loss coefficient time dependencies are presented in Fig. 8 for the four obtained capacitances under the source equivalent resistance 1 Ω. The graphics show that boost converter losses significantly depend on output capacitor value during the load transient. After the ending of the transient process, the maximum boost converter loss coefficients do not depend on the output capacitance significantly. The case of critical envelope mode (C=2.1 mF) shows the longest time during which the maximum loss coefficient is less than 10%. Very similar result is obtained by optimization procedure (C=1.94 mF). Thus, the boost converter efficiency can be increased by selection of output capacitance with accounting of estimated load transient processes duration.

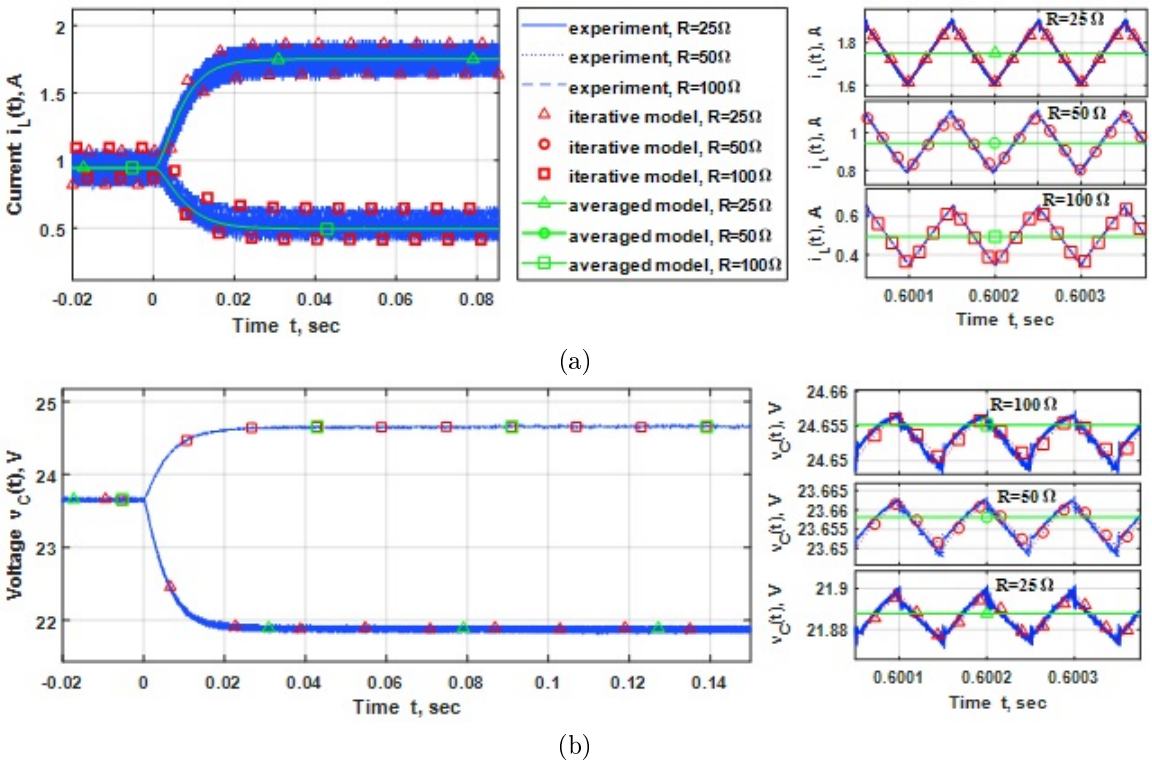

Рис. 7. The transient processes under optimized capacitance C=1.94 mF: (a) inductor currents; (b) output capacitor voltages

Table 2 Experimental and modeled losses and modelling relative errors for different boost converter transient modes

Transient Mode	C	Experiment	Iterative model			Averaged model		
		losses (47)	losses (47)	current error (49)	voltage error (49)	losses (47)	current error (49)	voltage error (49)
Critical for state 2 (30)	8,1 mF	14.26%	13.57%	1.10%	1.96%	13.39%	2.28%	1.42%
Maximum voltage boost (39)	40 μF	11.42%	11.28%	2.31%	1.83%	11.04%	2.86%	2.52%
Critical envelope (43)	2.1 mF	9.08%	9.23%	1.58%	1.31%	9.12%	1.84%	1.78%
Optimized (48)	1.94 mF	9.31%	9.12%	1.76%	1.25%	9.17%	1.65%	2.03%

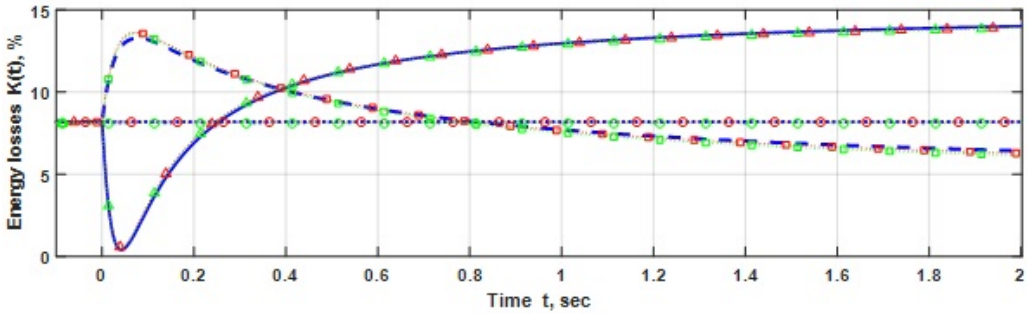

(a)

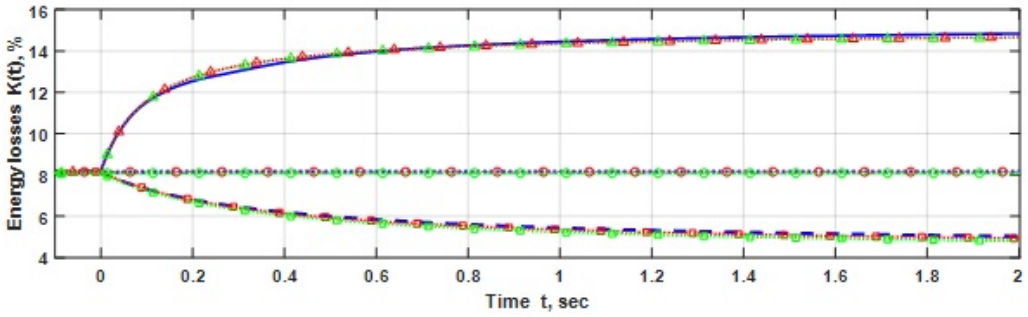

(b)

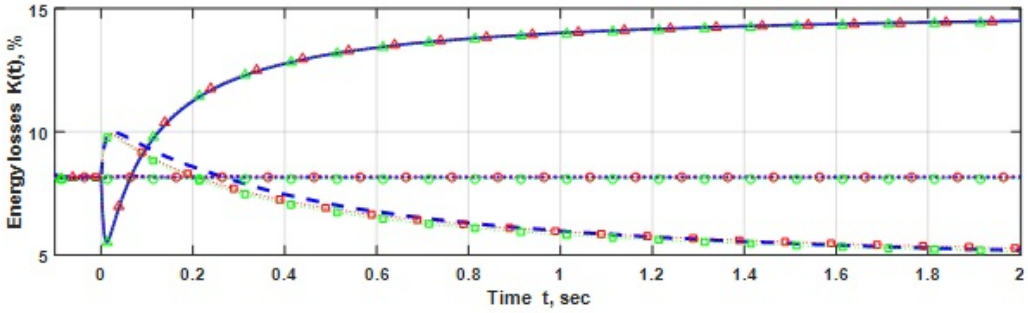

(c)

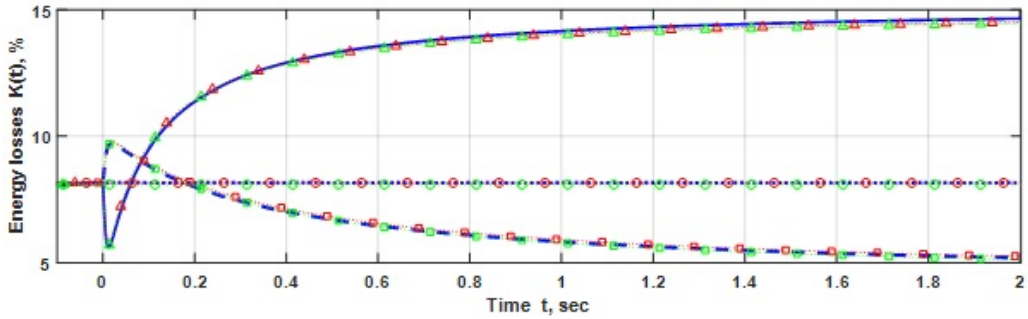

(d)

Рис. 8. Energy losses in different modes: (a) critical state 2, C=8 mF; (b) maximum voltage boost, C=40 µF; (c) critical envelope, C=2.1 mF; (d) optimized, C=1.94 mF

Conclusions

The boost converter efficiency (energy losses) and transient processes are analyzed for four different modes: critical mode of switch-off state, maximum voltage boost mode, critical averaged envelope mode and optimized mode. These modes are characterized by different energy losses during transient processes caused by load varying.

The first mode is given by the condition of critical transient process (between periodic and aperiodic modes) for the state 2 (switch-off). This transient mode appears under a great value of the circuit time constant, thus, it requires a great value of output capacitance. Such mode allows minimization of the losses during state 2. But the main disadvantage is that the state 1 transient processes are not taken into account. Thus, during the load transient process, energy loss is 14.26% under the state 2 critical mode.

The second mode is determined by the condition of maximum output voltage boost. In this case, the boost converter efficiency is higher. The losses are 11.42% during load transient process. The disadvantage of such mode is that the time-domain waveforms of transient processes are not taken into account. But this technique is useful, if the short-time load transient losses constraints are strict.

The third mode is obtained from the condition of critical transient process (between periodic and aperiodic modes) for averaged envelopes obtained by the state-space averaging method. Such transient process mode shows only 9.08% energy loss.

The fourth mode is obtained by using optimization procedure in MATLAB environment. The procedure is realized by MATLAB functions. The obtained result is closed to the critical transient process for the averaged envelope. The energy losses are 9.31%. The disadvantage of this technique is the presence of numerical calculation errors that appear in the optimization procedure.

The presented results show that different transient modes can be required for obtaining the best efficiency of energy transition under different load variation frequencies and durations. For example, if the load resistance changes for a short time, then maximum voltage boost mode is convenient with a small output capacitance which provides a short response time, as shown in Fig. 8 (b). But, if the load resistance changes for a longer time, then critical envelope mode (Fig. 8 (c)) is more efficient and provides a longer protection from high energy losses.

It should be noted that optimization procedure leads to parameters close to critical envelope mode. Probably, the minimum energy losses can be obtained in critical envelope mode. In such case, the difference between critical envelope mode parameters and optimization result can be caused by the calculation errors of boost converter models and optimization procedure.

Therefore, consideration of load transient process modes can provide a significant improvement of boost converter efficiency under varying load.

All modelling errors are lower than 3%, but the iterative model given by (2) and (3) does not match exactly with current and voltage ripples, because of the parasitic parameters that are not taken into account. Thus, for more exact boost converter ripples modelling, the more complex models should be used to fit the characteristics of semiconductor and passive elements. Especially, the investigation of fractional order capacitor models [40, 41] is interesting in accordance with greater capabilities of the ripple curves fitting without a significant increase of model parameters number.

References

[1] Williams B.W. (2008) Basic DC-to-DC Converters. *IEEE Transactions on Power Electronics*, Vol. 23, Iss. 1, pp. 387-401. DOI: 10.1109/tpel.2007.911829

[2] Forouzesh M., Siwakoti Y.P., Gorji S.A., Blaabjerg F. and Lehman B. (2017) Step-Up DC–DC Converters: A Comprehensive Review of Voltage-Boosting Techniques, Topologies, and Applications. *IEEE Transactions on Power Electronics*, Vol. 32, Iss. 12, pp. 9143-9178. DOI: 10.1109/tpel.2017.2652318

[3] Luo F.L. and Ye H. (2004) Advanced DC/DC Converters, CRC Press.

[4] Magaldi G.L., Serra F.M. and Silva L.I. (2015) Energy management control strategy for stand-alone photovoltaic system. *2015 XVI Workshop on Information Processing and Control (RPIC)*. DOI: 10.1109/rpic.2015.7497119

[5] Khan FH. Modular DC-DC converters. ProQuest Diss Theses 2007;Ph.D.

[6] Williams B.W. (2014) Generation and Analysis of Canonical Switching Cell DC-to-DC Converters. *IEEE Transactions on Industrial Electronics*, Vol. 61, Iss. 1, pp. 329-346. DOI: 10.1109/tie.2013.2240633

[7] Angelone G., Vasca F., Iannelli L. and Camlibel K. (2012) Dynamic and Steady-State Analysis of Switching Power Converters Made Easy: Complementarity Formalism. *Advances in Industrial Control*, pp. 217-243. DOI: 10.1007/978-1-4471-2885-4_7

[8] Rosas-Caro J.C., Mayo-Maldonado J.C., Valderrabano-Gonzalez A., Beltran-Carbajal F., Ramirez-Arredondo J.M. and Rodriguez-Rodriguez J.R. (2015) DC-DC multiplier boost converter with resonant switching. *Electric Power Systems Research*, Vol. 119, pp. 83-90. DOI: 10.1016/j.epsr.2014.09.003

[9] Ganesan R.G. and Prabhakar M. (2014) Non-isolated high step-up interleaved boost converter. *International Journal of Power Electronics*, Vol. 6, Iss. 3, pp. 288. DOI: 10.1504/ijpelec.2014.064654

[10] Çelebi M. (2018) Efficiency optimization of a conventional boost DC/DC converter. *Electrical Engineering*, Vol. 100, Iss. 2, pp. 803-809. DOI: 10.1007/s00202-017-0552-0

[11] Sai Krishna Reddy M., Kalyani C., Uthra M. and Elangovan D. (2015) A Small Signal Analysis of DC-DC Boost Converter. *Indian Journal of Science and Technology*, Vol. 8, Iss. S2, pp. 1. DOI: 10.17485/ijst/2015/v8is2/57787

[12] Ramu G., Nagesh Kumar G. V., Dharma Raj C.H. (2016) Performance Analysis of Boost Fed Dc Drive under Load Uncertainties. *Indian Journal of Science and Technology*, Vol. 9, Iss. 45. DOI: 10.17485/ijst/2016/v9i45/103878

[13] Beltrame F., Dupont F.H., Sartori H.C., Roggia L., Cancian E.C. and Pinheiro J.R. (2013) Different optimum designs investigation of DC/DC boost converter applied to the photovoltaic system. *2013 Brazilian Power Electronics Conference*. DOI: 10.1109/cobep.2013.6785167

[14] Eltamaly A.M. and Farh H.M. (2015) Smart maximum power extraction for wind energy systems. *2015 IEEE International Conference on Smart Energy Grid Engineering (SEGE)*. DOI: 10.1109/sege.2015.7324623

[15] Chen Y.-C., Chen C.-I. and Shao Z.-T. (2016) A DC-DC boost converter with high voltage gain for distributed generation. *2016 IEEE 5th Global Conference on Consumer Electronics*. DOI: 10.1109/gcce.2016.7800382

[16] Shi C., Miller B., Mayaram K. and Fiez T. (2011) A Multiple-Input Boost Converter for Low-Power Energy Harvesting. *IEEE Transactions on Circuits and Systems II: Express Briefs*, Vol. 58, Iss. 12, pp. 827-831. DOI: 10.1109/tcsii.2011.2173974

[17] Asadi F. and Eguchi K. (2018) Dynamics and Control of DC-DC Converters. *Synthesis Lectures on Power Electronics*, Vol. 6, Iss. 1, pp. 1-241. DOI: 10.2200/s00828ed1v01y201802pel010

[18] Marodkar M., Adhau S., Sabley M. and Adhau P. (2015) Design and simulation of DC-DC converters for Photovoltaic system based on MATLAB. *2015 International Conference on Industrial Instrumentation and Control (ICIC)*. DOI: 10.1109/iic.2015.7150983

[19] Li S., Attou A., Yang Y. and Geng D. (2015) A maximum power point tracking control strategy with variable weather parameters for photovoltaic systems with DC bus. *Renewable Energy*, Vol. 74, , pp. 478-488. DOI: 10.1016/j.renene.2014.08.056

[20] Panda R.K., Mohapatra A. and Srivastava S.C. (2016) A Lyapunov based controller for boost converter to integrate solar photovoltaic source. *2016 IEEE Innovative Smart Grid Technologies - Asia (ISGT-Asia)*. DOI: 10.1109/isgt-asia.2016.7796452

[21] Fermeiro J., Pombo J., Calado M. and Mariano S. (2017) A new controller for DC-DC converters based on particle swarm optimization. *Applied Soft Computing*, Vol. 52, pp. 418-434. DOI: 10.1016/j.asoc.2016.10.025

[22] Chan W.C.Y. and Tse C.K. (1998) What form of control function can drive a discontinuous-mode boost converter to chaos via period-doubling?. *International Journal of Circuit Theory and Applications*, Vol. 26, Iss. 3, pp. 281-286. DOI: 10.1002/(sici)1097-007x(199805/06)26:3<281::aid-cta10>3.0.co;2-0

[23] Furukawa Y., Nibu S., Colak I., Eto H. and Kurokawa F. (2016) Transient response of digital peak current mode boost converter for DC bus voltage compensation. *2016 IEEE International Conference on Renewable Energy Research and Applications (ICRERA)*. DOI: 10.1109/icrera.2016.7884448

[24] Chalermpol R. Y.K. and Chunkang V. (2014) Improve the transient response of DC/DC converter. *2014 International Electrical Engineering Congress (iEECON)*. DOI: 10.1109/ieecon.2014.6925833

[25] Ioinovici A. (1987) Exact transient solution of the boost converter computed using the alternor equations. *International Journal of Electronics*, Vol. 63, Iss. 5, pp. 767-772. DOI: 10.1080/00207218708939183

[26] Husna A.W.N., Siraj S.F. and Mat M.H. (2011) Effect of Load Variations in DC-DC Converter. *2011 Third International Conference on Computational Intelligence, Modelling & Simulation*. DOI: 10.1109/cimsim.2011.78

[27] Guo L., Hung J.Y. and Nelms R. (2011) Comparative evaluation of sliding mode fuzzy controller and PID controller for a boost converter. *Electric Power Systems Research*, Vol. 81, Iss. 1, pp. 99-106. DOI: 10.1016/j.epsr.2010.07.018

[28] Boora A.A., Zare F. and Ghosh A. (2011) A new family of multi-output DC-DC converter topologies to supply an asymmetrical four-level diode-clamped inverter. *COMPEL - The international journal for computation and mathematics in electrical and electronic engineering*, Vol. 30, Iss. 2, pp. 451-482. DOI: 10.1108/03321641111101023

[29] Liu M., Tse C.K. and Wu J. (2003) A wavelet approach to fast approximation of steady-state waveforms of power electronics circuits. *International Journal of Circuit Theory and Applications*, Vol. 31, Iss. 6, pp. 591-610. DOI: 10.1002/cta.252

[30] Middlebrook R.D. and Ćuk S. (1977) A general unified approach to modelling switching-converter power stages. *International Journal of Electronics*, Vol. 42, Iss. 6, pp. 521-550. DOI: 10.1080/00207217708900678

[31] Arjun M. and Patil V. (2015) Steady state and averaged state space modelling of non-ideal boost converter. *International Journal of Power Electronics*, Vol. 7, Iss. 1/2, pp. 109. DOI: 10.1504/ijpelec.2015.071204

[32] Chetty P.R.K. (1982) Current Injected Equivalent Circuit Approach to Modeling of Switching DC-DC Converters in Discontinuous Inductor Conduction Mode. *IEEE Transactions on Industrial Electronics*, Vol. IE-29, Iss. 3, pp. 230-234. DOI: 10.1109/tie.1982.356670

[33] Nwosu C.A. (2008) State-Space Averaged Modeling of a Nonideal Boost Converter. Pacific Journal of Science and Technology, Iss. 9, pp. 302–308.

[34] Rahman S. and Lee F. (1982) Computer Simulations of Optimum Boost and Buck-Boost Converters. *IEEE Transactions on Aerospace and Electronic Systems*, Vol. AES-18, Iss. 5, pp. 598-608. DOI: 10.1109/taes.1982.309272

[35] STW88N65M5 N-channel 650 V, 0.024 Ohm typ., 84 A MDmesh M5 Power MOSFET Technical Data n.d. https://www.st.com/en/power-transistors/stw88n65m5.html

[36] 30CPQ150 High Performance Schottky Rectifier, 2 x 15 A Technical Data n.d. https://www.vishay.com/docs/96455/vs-30cpq140-n3.pdf

[37] Kislovski A.S., Redl R. and Sokal N.O. (1991) *Dynamic Analysis of Switching-Mode DC/DC Converters*. DOI: 10.1007/978-94-011-7849-5

[38] Alonge F., Pucci M., Rabbeni R. and Vitale G. (2017) Dynamic modelling of a quadratic DC/DC single-switch boost converter. *Electric Power Systems Research*, Vol. 152, pp. 130-139. DOI: 10.1016/j.epsr.2017.07.008

[39] Chuang B. and Jingmei W. (2008) Discrete iterative mapping for the analysis of bifurcation and chaos in forward converter. *2008 International Conference on Communications, Circuits and Systems*. DOI: 10.1109/icccas.2008.4657965

[40] Chen X., Chen Y., Zhang B. and Qiu D. (2017) A Modeling and Analysis Method for Fractional-Order DC–DC Converters. *IEEE Transactions on Power Electronics*, Vol. 32, Iss. 9, pp. 7034-7044. DOI: 10.1109/tpel.2016.2628783

[41] Wang F.-Q. and Ma X.-K. (2011) Fractional order modeling and simulation analysis of Boost converter in continuous conduction mode operation. Acta Phys. Sin., Vol. 60, No 7, 070506.

Аналіз процесів передачі енергії у підвищуючому імпульсному перетворювачі

Мартинюк В. В., Косенков В. Д., Гейдарова О. В., Федула М. В.

Вступ. У статті описується аналіз процесів передачі енергії у підвищуючому перетворювачі за умов зміни навантаження. Досліджено лабораторний макет перетворювача при різних формах перехідного процесу, викликаного зміною навантаження. Перехідні струми і напруги виміряно в гармонічних і негармонічних режимах. Проведено оцінку параметрів перехідних режимів. Аналіз процесів переходу енергії здійснено за допомогою двох моделей підвищуючого перетворювача.

Постановка проблеми. Кола підвищуючих перетворювачів використовуються в областях електроніки, де мінімізація втрат енергії є критично важливою. Втрати енергії у підвищуючому перетворювачі залежать від форми перехідних процесів, викликаних зміною навантаження. Мінімізація втрат енергії вимагає точного аналізу процесів передачі енергії, які виникають при зміні навантаження. Запропонована робота описує реакції схеми перетворювача на зміни навантаження вдвічі з чотирма різними режимами перехідного процесу.

Результати. Аналіз процесів передачі енергії здійснюється з використанням двох моделей. Перша модель базується на методиці ітеративного відображення, де струми і напруги кожного періоду сигналу керування затвором транзистора визначаються за параметрами схеми і початковими умовами, заданими попереднім періодом керуючого сигналу. Така модель дозволяє проводити точний аналіз перехідних процесів і пульсацій струму та напруги. Проте, модель ітеративного відображення характеризується похибками числової апроксимації, і вимагає більше часу для виконання обчислень. Друга модель аналітично описує огинаючі перехідних процесів струму і напруги перетворювача. Така модель базується на методі усереднення у просторі станів, що широко використовується для моделювання імпульсних схем. Така модель не враховує форми пульсацій струмів і напруги, але забезпечує більш простий опис перехідних процесів, які корисні для цілей схемотехніки. Результати моделювання, отримані з ітеративного відображення та усереднення у просторі станів, співпадають з експериментальними даними, із відносною похибкою, яка не перевищує 3%.

Висновки. Проведений аналіз показує, що втрати енергії у підвищуючому перетворювачі залежать від перехідного процесу. Протягом перехідного процесу, викликаного зміною навантаження, найменші втрати енергії можуть бути отримані за умови критичної форми перехідного процесу, що розташована між гармонічним та негармонічним режимами. Такий результат отримано експериментально і підтверджено як ітераційним відображенням, так і моделями усереднення стану простору. Аналітичні результати підтверджуються процедурою оптимізації в середовищі MATLAB.

Ключові слова: підвищуючий імпульсний перетворювач; втрати енергії; перехідний процес; критичний режим; моделювання

Анализ процессов передачи энергии в повышающем импульсном преборазователе

Мартынюк В. В., Косенков В. Д., Гейдарова Е. В., Федула М. В.

Введение. В статье описывается анализ процессов передачи энергии в повышающем преобразователе при изменении нагрузки. Исследован лабораторный макет преобразователя при различных формах переходного процесса, вызванного изменением нагрузки. Переходные токи и напряжения измерены в гармонических и негармонических режимах. Проведена оценка параметров переходных режимов. Анализ процессов перехода энергии осуществлен с помощью двух моделей повышающего преобразователя.

Постановка проблемы. Цепи повышающих преобразователей используются в областях электроники, где минимизация потерь энергии является критически важной. Потери энергии в повышающем преобразователе зависят от формы переходных процессов, вызванных изменением нагрузки. Минимизация потерь энергии требует точного анализа процессов передачи энергии, которые возникают при изменении нагрузки. Предложенная работа описывает реакции схемы преобразователя на изменения нагрузки вдвое с четырьмя различными режимами переходного процесса.

Результаты. Анализ процессов передачи энергии осуществляется с использованием двух моделей. Первая модель основана на методике итеративного отображения, где токи и напряжения каждого периода сигнала управления затвором транзистора определяются по параметрам схемы и начальными условиями, заданными предыдущим периодом управляющего сигнала. Такая модель позволяет проводить точный анализ переходных процессов и пульсаций тока и напряжения. Однако, модель итеративного отображения характеризуется погрешностями числовой аппроксимации, и требует больше времени для выполнения вычислений. Вторая модель аналитически описывает огибающие переходных процессов тока и напряжения преобразователя. Такая модель базируется на методе усреднения в пространстве состояний, который широко используется для моделирования импульсных схем. Такая модель не учитывает формы пульсаций токов и напряжений, но обеспечивает более простое описание переходных процессов, полезное при разработке схемотехники. Результаты моделирования, полученные из итеративного отображения и усреднения в пространстве состояний, совпадают с экспериментальными данными, с относительной погрешностью, которая не превышает 3%.

Выводы. Проведенный анализ показывает, что потери энергии в повышающем преобразователе зависят от переходного процесса. В течение переходного процесса, вызванного изменением нагрузки, наименьшие потери энергии могут быть получены при критической форме переходного процесса, расположенной между гармоничным и негармоничным режимами. Такой результат получен экспериментально и подтвержден как итеративным отображением, так и моделями усреднения состояния пространства. Аналитические результаты подтверждаются процедурой оптимизации в среде MATLAB.

Ключевые слова: повышающий преобразователь; потери энергии; переходный процесс; критический режим; моделирование